

***para*-Nitroaniline-functionalized chromophoric organic–inorganic hybrid materials†**Katharina Ladewig,^{ab} Andreas Seifert,^a Harald Hahn,^a Michael Hietschold,^c Norbert Moszner,^d Peter Bartscher^d and Stefan Spange^{*a}

Received 24th October 2011, Accepted 16th December 2011

DOI: 10.1039/c2jm15407b

An advanced procedure for the one-pot synthesis of organic–inorganic hybrid materials *via* combination of sol–gel process and nucleophilic aromatic substitution reaction (S_NAr) of 4-fluoronitrobenzene and 3-aminopropyltrimethoxysilane is described. With this advanced procedure both S_NAr -reaction and sol–gel process can be accomplished in the same reaction vessel due to the sol–gel precursor tetraethoxysilane (TEOS) acting as solvent during the first reaction step. *Via* extensive NMR spectroscopic studies it is proven for the first time that—contrary to common belief—hydrogen fluoride (HF), which is formed as a by-product in the S_NAr -reaction, is not trapped by any bases present but is rather trapped by both of the silane species and serves as a catalyst during the subsequent sol–gel process. The chromophoric system of the resulting xerogels is well protected against aggressive chemicals, *i.e.* strong acids, by the silica matrix, which predestines these materials for pigment applications. Given that a high chromophore content is highly desirable in these applications, we show that the chromophore content of the final xerogel can be varied by modification of the organosilicon precursor : TEOS ratio or by using trialkoxy-silanes bearing two or three amino functions, whereby the latter option is more favourable. Monodisperse core–shell particles with identical chromophore content but consisting of a pure silica-core and a *p*-nitroaniline functionalized shell with a diameter of about 200 nm can also be prepared using this advanced procedure.

Introduction

Coloured organic–inorganic hybrid materials find application in many fields, but most particularly in a variety of optical and sensing applications or in the pigment industry.^{1–17} Generally, they are comprised of organic chromophores, *i.e.*, organic dyes, and an inorganic, structure- and property-determining matrix. According to Sanchez's classification of hybrid materials,⁵ there are two modalities by which an organic dye can be attached to an inorganic matrix, *via* encapsulation (type I) or covalent linkages (type II). Hybrid materials of the former type are readily

available by dissolution of the desired dye in one of the components required for the sol–gel process prior to initiation of gelation. However, this purely physical/sterical interaction between the dye and matrix means that encapsulated dyes can be extracted by solvents or can be attacked by contaminants causing loss and/or degradation of the chromophore with time. Therefore, most applications utilize type II hybrid materials, simply because the organic component (dye) is protected from external influences such as organic solvents and/or other aggressive compounds. For the preparation of such materials functional alkyl alkoxysilanes with covalently tethered chromophores are required. The synthesis of those compounds is laborious, time consuming, and expensive.^{1–17}

Recently, we described an alternative experimental procedure for the synthesis of such class II hybrid materials, which combines the nucleophilic aromatic substitution (S_NAr) reaction of fluoro-aromatic compounds and aminofunctionalized trialkoxysilanes with a consecutively occurring sol–gel process in the presence of tetraethoxysilane (TEOS) and in some cases a base in a very convenient one-pot synthesis.^{18–21} The reaction concept is illustrated in Scheme 1. The S_NAr reaction of fluoro-aromatic hydrocarbons such as 4-fluoronitrobenzene (4-FNB) with primary or secondary aminotrialkoxysilanes results in the formation of a chromophoric push–pull system if the substituent

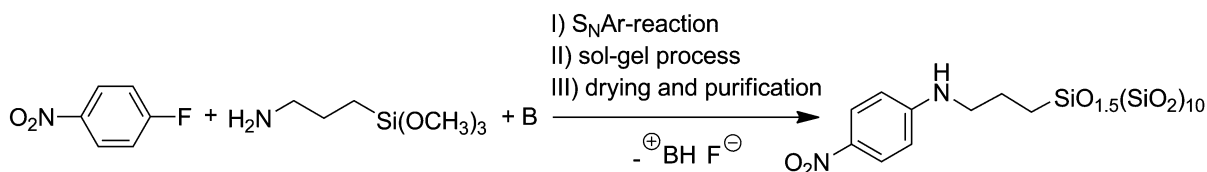
^aInstitute of Chemistry, Chemnitz University of Technology, Strasse der Nationen 62, D-09111 Chemnitz, Germany. E-mail: stefan.spange@chemie.tu-chemnitz.de

^bDepartment of Chemical and Biomolecular Engineering, The University of Melbourne, Parkville, VIC, 3010, Australia. E-mail: katharina.ladewig@unimelb.edu.au

^cInstitute of Physics, Chemnitz University of Technology, Strasse der Nationen 62, D-09111 Chemnitz, Germany

^dIvoclar Vivadent AG, Bendererstrasse 2, FL-9494 Schaan, Liechtenstein

† Electronic supplementary information (ESI) available: Eqn (S1): mathematical equation for the calculation of ϵ ; Fig. S1: UV/Vis spectra of heat-treated xerogels; Fig. S2: plot of λ_{max} of solubilized *p*-nitroaniline functionalized xerogels *vs.* pH; Fig. S3 and S4: ¹³C-¹H-CP-MAS NMR spectra of DAS- and TAS-derived xerogels. See DOI: 10.1039/c2jm15407b



Scheme 1 Synthetic procedure for the preparation of chromophoric xerogels. The yellow coloured *N*-(3-trimethoxysilylpropyl)-*para*-nitroaniline chromophore is formed through the nucleophilic aromatic substitution (S_NAr) reaction of 4-fluoronitrobenzene (4-FNB) and 3-amino-propyltrimethoxysilane (APS) in tetraethoxysilane (TEOS) as solvent using an external base B, *i.e.*, *N,N*-dimethyl-*n*-octylamine (step I). The final product is obtained after initiation of the sol-gel process with water and controlled aging of the gel (step II), drying and purification by Soxhlet extraction (step III).

in *para*- or *ortho*-position to the fluorine atom is strongly electron withdrawing.²²

Since TEOS acts as a solvent in this first step, no additional solvent (*i.e.*, alcohol) is required for the S_NAr reaction and the consecutive sol-gel process can be accomplished in the same reaction vessel. In recent papers we demonstrated that this concept works well for the immobilization of a broad variety of molecular structures of chromophores.^{18–21} However, some open questions remained, namely (i) the role of fluoride during the S_NAr reaction, (ii) the extent to which the intermediate product—the chromophore—is incorporated into the final product, (iii) whether the xerogel syntheses are suitably reproducible, (iv) the xerogels are stable to thermal and/or other external stimuli, and (v) whether it is possible to increase the dye content and if so how. The HF formed during the S_NAr reaction is thought to serve as catalyst during the sol-gel process, hence may not need to be removed or trapped by a base (*e.g.*, tertiary amine). However, its role during this first step of the synthesis process, the S_NAr reaction, and its catalyzing effect on the sol-gel process in this particular system are not fully understood and need to be elucidated further. As shown in previous publications, the colour and other physicochemical properties of the produced materials can be adjusted in a wide range by variation of the fluoro-compound and/or the synthesis conditions.^{18–21} However, their application as pigments also calls for highly stable xerogels, which are able to withstand a variety of chemical and mechanical stresses, while at the same time maximum colour intensity needs to be realisable in blends using minimal quantities of these materials. In this manuscript we systematically study the role of HF, the thermal and pH-stability of as-synthesized xerogels as well as ways to achieve particle monodispersity and the different means by which the colour intensity can be increased.

Experimental section

Materials

APS (97%, Lancaster), TEOS (98%, Acros Organics), *N,N*-dimethyl-*n*-octylamine (DMOA) and pyridine were distilled under reduced pressure and stored in dry argon atmosphere prior to use. *N*-Propylamine (99%, Acros Organics), 3-(2-aminoethylamino)propyltrimethoxysilane (DAS, >98%, Fluka), (3-trimethoxysilylpropyl)diethylenetriamine (TAS, 95%, ABCR), trimethylmethoxysilane (95%, ABCR), hexamethyldisiloxane (>98%, Alfa Aesar), *N*-propylethylenediamine (99%, Acros Organics) and diethylenetriamine (>98%, Merck) were used as received. *N,N*-Dimethyl-*n*-octylammonium fluoride (DMOAF)

was synthesized from DMOA and hydrofluoric acid and vacuum-dried over phosphorus pentoxide prior to use.

Synthesis of *p*-nitroaniline functionalized xerogels

One-pot synthesis method. *N*-(3-Trimethoxysilylpropyl)-*para*-nitroaniline (*p*NA) functionalized xerogel syntheses were performed following the two different pathways described in Scheme 3. Isolation of the product was achieved by rotary evaporation at 70 °C and 15 mbar, followed by further dewatering using a rotary furnace (7 h at 70 °C and 0.1 mbar), Soxhlet extraction with acetone (64 h) and finally drying of the product until constant weight in a vacuum drying cabinet at 40 °C. DAS- and TAS-derived *p*NA-functionalized xerogels were synthesized according to pathway B (Scheme 3).

Core-shell particles. 1.5 L ethanol, 120 mL ammonia (25%), 7.1 mL water and 74.4 mL (367.9 mmol) TEOS are stirred for five hours at room temperature to give the silica core of the final product (Stöber particles). 5.19 g (36.8 mmol) 4-FNB, 7.71 g (37.0 mmol) TEOS and 6.85 g (38.2 mmol) APS are stirred for 5.5 hours at 150 °C under inert argon atmosphere and mixed with 20 mL pure ethanol after cooling down to room temperature. The yellow solution is added to the Stöber particles under vigorous stirring. Ammonia and ethanol are removed under reduced pressure after 16 hours of stirring and a yellow coloured powder is obtained. Further processing was performed as for the other xerogels.

Synthesis of M1 ([*N*-propyl]-4-nitroaniline)

2.26 g (16.0 mmol) 4-FNB was added to 20 mL of cold (−18 °C) *n*-propylamine. After 10 minutes 2.4 mL (17.2 mmol) trimethylmethoxysilane was added and the mixture was heated to 60 °C for one hour. The solvents were removed under vacuum at 110 °C to give the pure product in 95% yield with a melting point of 62 °C. ¹H NMR (250 MHz, δ , ppm, CDCl₃) = 8.08 (2H, m), 6.51 (2H, m), 4.5 (1H, s, broad), 3.18 (2H, ³*J*(¹H–¹H) = 7.1 Hz, ³*J*(¹H–¹H_{NH}) = 5.6 Hz), 1.69 (2H, tq, ³*J*(¹H–¹H) = 7.4 Hz, ³*J*(¹H–¹H) = 7.1 Hz), 1.02 (3H, t, ³*J*(¹H–¹H) = 7.4 Hz). ¹³C-{¹H} NMR (62.5 MHz, δ , ppm, CDCl₃) = 153.4, 137.8, 126.5, 110.9, 45.1, 22.4, 11.5.

Synthesis of M2 ([*N*1,*N*2-bis(4-nitrophenyl)-*N*1-propylethane-1,2-diamine])

3.18 g (22.4 mmol) 4-FNB, 0.58 g (5.6 mmol) *N*-propylethylenediamine and 1.44 g (13.8 mmol) trimethylmethoxysilane were

refluxed at 160 °C for 34 h. Ethanol was added to the mixture and the yellow-brown coloured solid was filtered off and again boiled with ethanol and filtered off. Yellow needles with a melting point of 176–178 °C in a yield of 25% were obtained. ^1H NMR (250 MHz, δ , ppm, d_6 -DMSO) = 8.00 (4H, m), 7.34 (1H, t, $^3J(\text{H}-\text{H}) = 6.0$ Hz, *NH*), 6.79 (2H, m), 6.66 (2H, m), 3.65 (2H, t, $^3J(\text{H}-\text{H}) = 6.5$ Hz), 3.39 (4H, m), 1.56 (2H, m), 0.88 (3H, t, $^3J(\text{H}-\text{H}) = 7.3$ Hz). ^{13}C - $\{^1\text{H}\}$ NMR (62.5 MHz, δ , ppm, d_6 -DMSO) = 154.6, 153.0, 136.2, 135.8, 126.5, 126.3, 110.9, 52.5, 49.4, 39.9, 20.0, 11.2.

Synthesis of M3 (1*N*1,2*N*3-tris(4-nitrophenyl)-diethylenetriamine)

1.36 g (13.2 mmol) diethylenetriamine, 5.57 g (39.5 mmol) 4-FNB and 2 mL hexamethyldisiloxane were refluxed for 5 h at 140 °C, 20 h at 150 °C and 10 h at 190 °C. The crude product was dissolved in DMSO, precipitated by addition of ethanol and filtered off. The procedure was repeated six times to obtain a light brown powder with a melting and decomposition temperature of 269–270 °C in 36% yield. ^1H NMR (250 MHz, δ , ppm, d_6 -DMSO) = 8.05 (2H, m), 7.95 (4H, m), 7.34 (2H, t, $^3J(\text{H}-\text{H}) = 5.8$ Hz), 6.85 (2H, m), 6.62 (4H, m), 3.66 (4H, t, $^3J(\text{H}-\text{H}) = 6.4$ Hz), 3.42 (4H, dt ($^3J(\text{H}-\text{H}) = 6.4$ Hz); $^3J(\text{H}-\text{H}) = 5.8$ Hz). ^{13}C - $\{^1\text{H}\}$ NMR (62.5 MHz, δ , ppm, d_6 -DMSO) = 154.5, 152.9, 136.3, 136.2, 126.5, 126.3, 111.2, 49.9, 39.7.

Characterization

NMR spectroscopic measurements. Solid state NMR spectra were collected at 9.4 T on a Bruker Avance 400 spectrometer equipped with double-tuned probes capable of MAS (magic angle spinning). ^{13}C - $\{^1\text{H}\}$ -CP-MAS NMR spectra were measured at 100.6 MHz in 4 mm standard zirconium oxide rotors (BRUKER) spinning at 12 kHz. Cross-polarization with a contact time of 5 ms was used to enhance the sensitivity. The recycle delay was 4 s. Spectra were referenced externally to tetramethylsilane (TMS) as well as to adamantane as secondary standard (38.48 ppm for ^{13}C). ^{23}Si - $\{^1\text{H}\}$ -CP-MAS NMR spectroscopy was performed at 79.5 MHz using 7 mm rotors spinning at 5 kHz. The contact time was 3 ms and the recycle delay 3 s. Shifts were referenced externally to tetramethylsilane (0 ppm) with the secondary standard being tetrakis(trimethylsilyl)silane (−9.8, −135.2 ppm). All spectra were collected with ^1H decoupling using a TPPM pulse sequence. ^1H decoupled quantitative ^{29}Si - $\{^1\text{H}\}$ -MAS NMR spectra were collected with 70° rf pulses and recycle delays of 300 s. 24 Decomposition of individual signals was performed using DMFit software provided by Massiot *et al.* 25

UV/Vis spectroscopic measurements. UV/Vis absorption spectra were collected using a UV/Vis MCS 400 diode-array spectrometer (Carl Zeiss, Jena) connected to a diffuse reflectance accessory cell *via* glass-fiber optics. Solutions were measured by the transmission technique using quartz cuvettes with an optical pathway length of 2 mm.

Electron microscopy. Scanning electron micrographs (SEMs) were recorded on a Philips SEM 515 instrument. Prior to

imaging, gold was evaporated onto the samples to render them electrically conductive. Transmission electron microscopy (TEM) was performed using a Philips CM 20 FEG microscope with the samples being fixed on carbon grids.

Thermogravimetry. TG measurements were performed in air between 40 and 900 °C at a heating rate of 10 K min $^{-1}$ using a Thermogravimetric Analyser 7 (Perkin Elmer).

Specific surface area. Nitrogen adsorption isotherms were measured at 77.3 K using a Sorptomatic 1900. Specific surface areas were calculated using the Brunauer–Emmett–Teller (BET) approximation. Single point measurements were performed on an Areameter II setup (Söhnle Instruments).

Results and discussion

$\text{S}_{\text{N}}\text{Ar}$ reaction of 4-FNB and aminofunctionalized trialkoxysilanes

The use of TEOS as both solvent during the $\text{S}_{\text{N}}\text{Ar}$ reaction of fluoro-aromatic compounds with aminosilanes and precursor for the subsequently induced sol–gel process is the key feature of our previously described one-pot synthesis method. $^{18-21}$ Tetraalkoxysilanes are solvents of moderate polarity whereas nucleophilic aromatic substitutions of amines with fluoro-aromatic compounds succeed in polar solvents such as dimethyl sulfoxide or pyridine. $^{26-28}$ Selective combinations of solvent mixtures and additional bases were studied in order to elucidate the influence of both polarity and basicity of the environment on the conversion of APS with 4-FNB. The progress of individual reactions was observed by ^1H NMR spectroscopy.

Firstly, pure chromophoric *N*-(3-trimethoxysilylpropyl)-*para*-nitroaniline (*p*NA) was synthesized *via* the reaction of 4-FNB and APS at 100 °C in freshly distilled pyridine as described by Claude *et al.* 29 Complete conversion was achieved after 4 h. As shown in Fig. 1 multiple signal sets are found in the ^1H and ^{13}C - $\{^1\text{H}\}$ NMR spectra for both the methoxy groups of the $(\text{CH}_3\text{O})_3\text{Si}$ moiety and the methylene group adjacent to the silicon atom.

This result was wholly reproducible even when the reactions were performed under absolutely water-free and inert conditions. Additionally, the number of hydrogen signals observed for the anticipated $(\text{CH}_3\text{O})_3\text{Si}$ moiety is less than nine. These observations indicate that a substitution reaction occurs at the silicon atom. Theoretically, one molecule of HF is liberated for each *p*NA molecule formed. As suggested previously, 30 this can lead to fluorine substitution at the silicon atom of both the product and starting reagent APS (Scheme 2).

According to Tacke *et al.* the substitution reaction occurs *via* a zwitterionic, pentavalent silicon species, $^{31-34}$ and methanol formed by either APS or *p*NA is readily detectable using various suitable methods such as gas chromatography or ^1H NMR spectroscopy, a fact not considered by Claude *et al.* 29 Further, we observed that the equimolar reaction between 4-FNB and APS in the substance without pyridine takes place quantitatively. This indicates that the HF formed is not trapped by APS *via* an acid–base reaction that forms ammoniumpropyltrimethoxysilane fluoride, because if this is the case the reaction would only

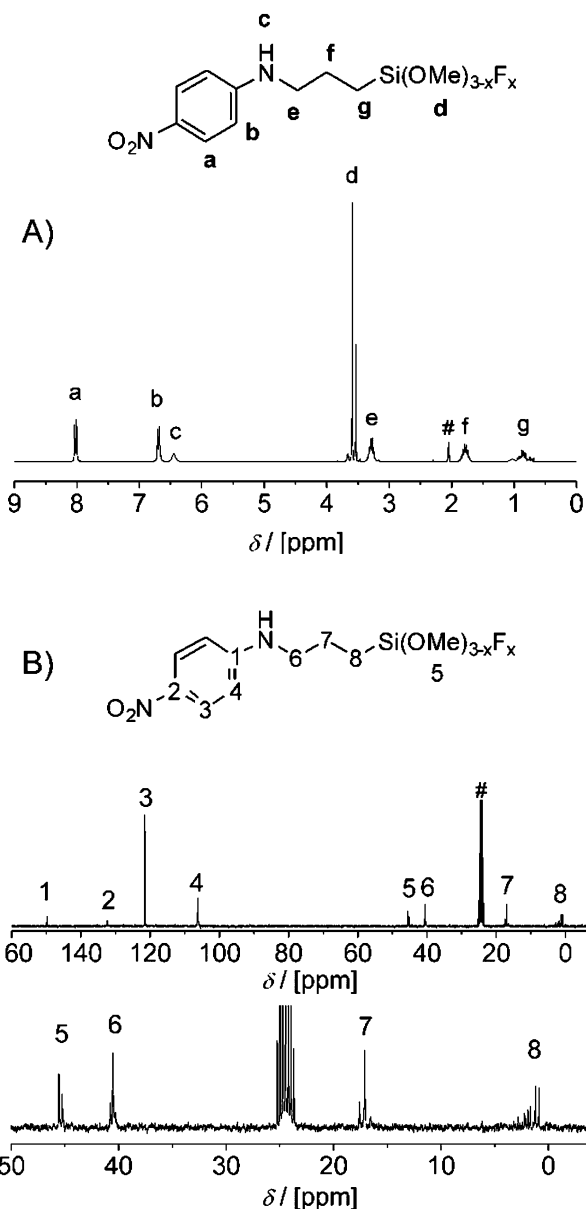
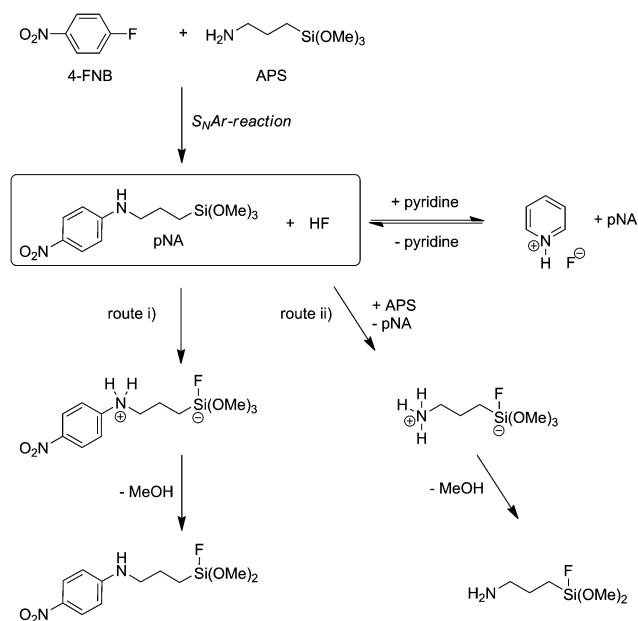


Fig. 1 (A) ¹H and (B) ¹³C-{¹H} NMR spectra and peak assignment for the anticipated product, *N*-(3-trimethoxysilylpropyl)-*para*-nitroaniline (*pNA*), of the *S_NAr*-reaction between 4-fluoronitrobenzene (4-FNB) and 3-aminopropyltrimethoxysilane (APS) [reaction in pyridine at 100 °C, spectra measured in *d*₆-acetone (#)].

proceed to 50% since the remaining APS would be fully protonated at this point and the formed ammonium hydrogen fluoride is not capable of *S_NAr* reactions. In short, the formed HF cannot be trapped by any bases for the reason that acid–base reactions are equilibrium reactions while the formation of fluoro-silanes is not. It can therefore be concluded that any HF that is formed as the reaction progresses does indeed react further with any of the alkoxy silane species present in the reaction mixture (routes (i) and (ii) in Scheme 2).

Secondly, the reaction of APS and 4-FNB was carried out using TEOS as the solvent. Changing the solvent from pure pyridine to TEOS slows down the reaction rate considerably, with reaction times of 20 h or more and temperatures as high as



Scheme 2 *S_NAr*-reaction of 4-FNB with APS forming *N*-(3-trimethoxysilylpropyl)-*para*-nitroaniline (*pNA*) in pyridine as solvent, and possible subsequent reactions of *pNA* (route i) and APS (route ii) with hydrogen fluoride that is formed during the *S_NAr*-reaction.

150 °C being necessary before 90% conversion of the reactants is achieved. Hence, we investigated the influence of a variety of experimental parameters, *e.g.*, molar ratios, temperatures, and additional bases, on the reaction rate. Namely pyridine and the stronger base *N,N*-dimethyl-*n*-octylamine (DMOA) were used in approximately equimolar concentrations to 4-FNB to accelerate the conversion. Time conversion plots for the various reaction parameters studied are displayed in Fig. 2. From the plots it can be concluded that the addition of external bases to the reaction mixture is not really necessary (compare runs 1, 2 and 3), since the increase in reaction rate is almost outweighed by the slowing effect the lowered educt concentrations (due to the addition of the base) have on the reaction rate. Surprisingly pyridine was observed to have a considerably stronger effect on the reaction

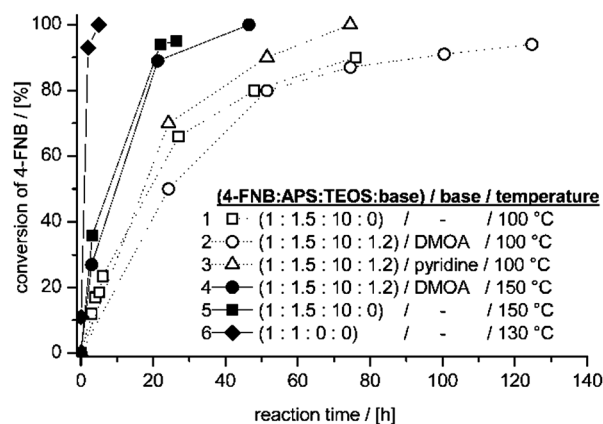


Fig. 2 Progress of the *S_NAr*-reaction of 4-FNB with APS as a function of time under various reaction conditions [TEOS: tetraethoxysilane, DMOA: *N,N*-dimethyl-*n*-octylamine, ratios given refer to molar ratios of the compounds; lines are a guide for the eye of the reader only].

rate than DMOA, even though it is a weaker base (compare runs 2 and 3). Having a ten-fold excess of TEOS in the reaction mixture slows down the reaction rate so significantly that 90% conversion of the reagents is only achieved after more than 20 h of refluxing the reaction mixture at 150 °C (runs 4 and 5). In contrast, the reaction of 4-FNB and APS in the substance (without TEOS) at 130 °C is completed within three hours (run 6).

However, omitting the TEOS completely renders the reaction mixture quite difficult to handle due to the formation of sublimates and causes inconsistent results. Thus, we decided on an equimolar ratio of 4-FNB, APS, and TEOS for the first reaction step, the S_NAr -reaction. After complete conversion of the reactants is achieved with certainty, *i.e.*, after five hours at 150 °C, the remaining nine equivalents of TEOS are added to the mixture and the sol-gel process is initiated. A $^{29}\text{Si}\{-^1\text{H}\}$ NMR spectrum of the reaction mixture just prior to the addition of the remaining nine equivalents of TEOS reveals many different silicon species originating from the variety of substitution reactions that HF can undergo with TEOS and APS. We were able to assign all observed signals to their corresponding molecular structure element by $^1\text{H}\text{--}^{29}\text{Si}$ NMR correlation experiments (Table 1).

The occurrence of various signals attributable to mixed alkoxy silane species clearly indicated that apart from the substitution

reactions the formed HF can undergo with the alkoxy silanes, they also undergo substitution reactions amongst themselves, probably catalyzed by the presence of the fluoride ions.

Si-C bond cleavage as observed by Moreau *et al.*³⁵ for the S_N2 -reaction of chloromethyltrimethoxysilane with amines was not observed. After reaction of a 1 : 1 mixture of APS and 4-FNB for 5 h at 150 °C to give the *p*NA product and subsequent initiation of the sol-gel process only T-signals and no Q-signals were found in the $^{29}\text{Si}\{-^1\text{H}\}$ -CP-MAS NMR spectra of the xerogel which corroborates our conclusion that all Si-C bonds survived the reaction.

Effect of HF on gelation times

Fluoride ions are known to be very effective sol-gel catalysts since they strongly influence both the hydrolysis and the condensation reactions of alkoxy silanes.^{36–39} The effect of the fluoride concentration on the gelation time was studied using a model system consisting of APS and TEOS (in a molar ratio of 1 : 10) and the model fluoride *N,N*-dimethyl-*n*-octylammonium fluoride (DMOAF). The model fluoride was dissolved in ethanol (equivalent to three times the amount of water used to start the sol-gel process; $n_{\text{EtOH}} = 3n_{\text{water}}$) and subsequently added to the TEOS-APS mixture. Gelation times were measured from the moment water (equimolar to all hydrolysable Si-OR bonds; $n_{\text{water}} = 3n_{\text{APS}} + 4n_{\text{TEOS}}$) was added to the mixtures containing various amounts of DMOAF until the initially clear solutions appeared cloudy. As shown in Table 2 gelation occurred after approximately 15–18 min in the reference experiment without DMOAF (run 1), whilst concentrations of fluoride below 1 ppm were already able to halve this time to about 8 min (run 4). A further increase of the fluoride concentration resulted in gelation times as short as one second (run 7). However, it is undesirable that the gelation occurs too fast since this can result in inhomogeneities in the final xerogel. One simple means of prolonging gelation times is to increase the ethanol amount used for the sol-gel process (runs 6, 6a, and 6b). Based on the discussed experiments an ethanol to water ratio of 10 : 1 was deemed most appropriate for the xerogel syntheses.

Synthesis and characterization of *p*-nitroaniline functionalized xerogels

Having derived the optimum conditions for both S_NAr -reaction and sol-gel process the reproducibility of xerogel syntheses was

Table 1 Silicon species found in the reaction mixture of 4-FNB, APS, and TEOS after five hours at 130 °C as determined by liquid $^{29}\text{Si}\{-^1\text{H}\}$ NMR spectroscopy in d_6 -acetone

Silicon species ^a	^{29}Si chemical shift	Coupling constants
R-Si(OMe) ₃	−42.6 ppm	
R-Si(OMe) ₂ (OEt)	−43.8 ppm	
R-Si(OMe)(OEt) ₂	−45.0 ppm	
R-Si(OEt) ₃	−46.2 ppm	
R-SiF(OMe) ₂	−46.8 ppm	$^1J(^{29}\text{Si}\text{--}^{19}\text{F}) = 272.2 \text{ Hz}$
R-SiF(OMe)(OEt)	−47.8 ppm	$^1J(^{29}\text{Si}\text{--}^{19}\text{F}) = 272.4 \text{ Hz}$
R-SiF(OEt) ₂	−48.9 ppm	$^1J(^{29}\text{Si}\text{--}^{19}\text{F}) = 272.6 \text{ Hz}$
Si(OMe) ₄	−78.5 ppm	
Si(OMe) ₃ (OEt)	−79.4 ppm	
Si(OMe) ₂ (OEt) ₂	−80.3 ppm	
Si(OMe)(OEt) ₃	−81.2 ppm	
Si(OEt) ₄	−82.1 ppm	
SiF(OMe) ₃	Not observed	
SiF(OMe) ₂ (OEt)	−86.8 ppm	$^1J(^{29}\text{Si}\text{--}^{19}\text{F}) = 195.4 \text{ Hz}$
SiF(OMe)(OEt) ₂	−87.6 ppm	$^1J(^{29}\text{Si}\text{--}^{19}\text{F}) = 196.3 \text{ Hz}$
SiF(OEt) ₃	Not observed	

^a R = $(\text{CH}_2)_3\text{NHC}_6\text{H}_4(p\text{-NO}_2)$.

Table 2 Gelation times of 1 : 10 molar mixtures of APS and TEOS after addition of water as a function of fluoride concentration (DMOAF) in ethanol as solvent. Water was used in an equimolar ratio to the number of Si-OR groups present in the mixture

#	Mole fraction of fluoride ^a /ppm	Molar ratio EtOH : water ^b	Molar ratio silicon : fluoride	Gel time
1	0	3 : 1	1 : 0	15–18 min
2	0.008	3 : 1	7 000 000 : 1	12–14 min
3	0.04	3 : 1	140 000 : 1	11–12 min
4	0.08	3 : 1	70 000 : 1	8–8.5 min
5	24	3 : 1	2500 : 1	50 s
6	107	3 : 1	560 : 1	30 s
6a	55	7 : 1	560 : 1	80 s
6b	25	17 : 1	560 : 1	23 min
7	1130	3 : 1	55 : 1	1 s

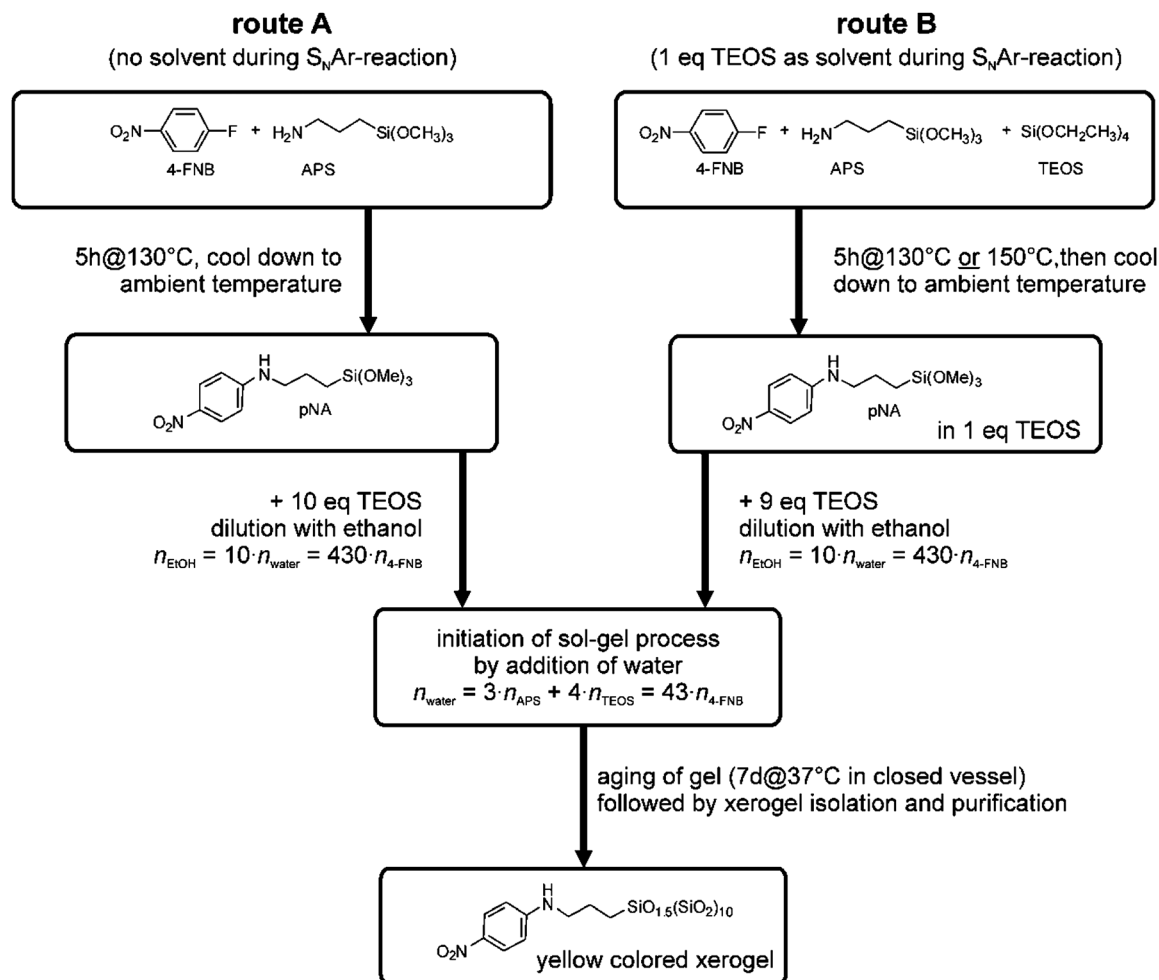
^a Mole fraction of fluoride (DMOAF) = $n_{\text{DMOAF}}/(n_{\text{DMOAF}} + n_{\text{APS}} + n_{\text{TEOS}} + n_{\text{water}} + n_{\text{EtOH}})$. ^b $n_{\text{water}} = 3n_{\text{APS}} + 4n_{\text{TEOS}}$.

tested next. Scheme 3 explains the two variations of the synthesis procedure used for this purpose. Despite the benefits an excess of APS can have on the conversion rate of the S_NAr -reaction equimolar ratios of 4-FNB and APS were employed during all xerogel syntheses since the primary amino-groups of non-reacted APS can have a negative effect in subsequent applications of these xerogels, *e.g.*, if they are to be used as fillers in reactive polymer systems cured *via* radical polymerization. Therefore, removal of any 4-FNB remaining after xerogel synthesis *via* Soxhlet-extraction is preferred, because it occurs quantitatively.

By means of the two procedures shown in Scheme 3 a series of *p*-nitroaniline-functionalized xerogels was synthesized. The simplest way to verify the reproducibility of xerogel syntheses is to weigh the final product and determine the yield of the reaction. However, the catch here is that the exact molecular weight of the final xerogel is unknown. The “idealized” structure of the product as depicted in Scheme 1 has a molecular weight of $832.15 \text{ g mol}^{-1}$, but this value is based on the assumption that all Si-OR bonds are hydrolyzed and all Si-OH groups are condensed during the reaction, and the xerogel does not contain any impurities such as residual solvent or water. The graph displayed in Fig. 3 illustrates the relationship between the mass of xerogel obtained and the feed amount of 4-FNB during our experiments.

The linear correlation of these two values indicates very good reproducibility of the synthetic process. The slope of the linear regression was determined to be $850.09 \text{ g mol}^{-1}$, which represents the “real” molecular weight of the formed xerogels. This slightly larger value than the “ideal” molecular weight indicates that either the sol-gel process or the S_NAr -reaction does not proceed to complete conversion or there may be a loss of the organic chromophore during the long extraction procedure with acetone. Quite possibly a combination of all three of the above mentioned reasons causes the observed difference between “ideal” and “real” molecular weight of the xerogels.

Solid state $^{29}\text{Si}\{-^1\text{H}\}$ -CP-MAS NMR measurements revealed the presence of Q_2 - and Q_3 -signals in the spectra of all xerogels, which clearly indicates the incomplete hydrolysis and condensation of the ethoxy groups of TEOS (Fig. 4A). This type of sensitivity enhanced NMR experiment uses a cross-polarization (CP) technique to transfer the magnetization from ^1H to ^{29}Si nuclei; hence signals of silicon species which are in close proximity to protons are particularly amplified. As a result T -, Q_2 - and Q_3 -signals are overestimated, while Q_4 -signals which originate from completely condensed silicon species are underestimated. In contrast, quantitative solid state $^{29}\text{Si}\{-^1\text{H}\}$ -MAS NMR spectra reflect the exact composition of the xerogel more



Scheme 3 Illustration of the different synthesis pathways employed.

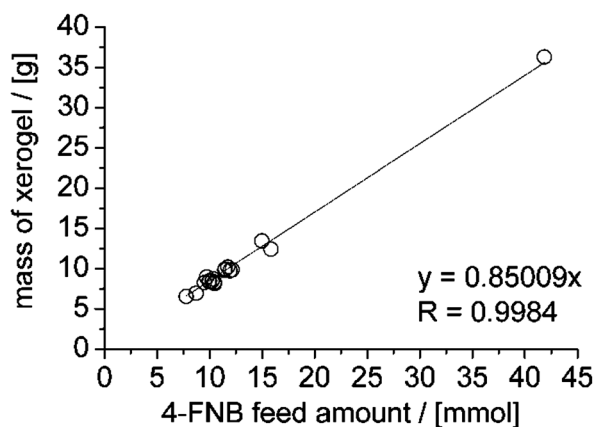


Fig. 3 Mass of xerogel obtained as a function of the feed amount of 4-FNB. The linear correlation verifies synthesis reproducibility, while the slope can be used to determine the apparent molecular weight of *p*-nitroaniline (*p*NA) functionalized xerogels [$n = 18$ syntheses according to procedures A (4 syntheses) and B (14 syntheses) as shown in Scheme 3].

accurately, but at the cost of longer measuring times. As shown in Fig. 4B the signals for the T_2 - as well as the Q_2 -silicon species all but vanished in the quantitative spectrum since their mole fractions are far below 0.5 mol%. Furthermore, the non-sensitivity enhanced $^{29}\text{Si}\{-^1\text{H}\}$ -MAS NMR spectrum showed a weak signal at about -175 ppm which was not observable in the $^{29}\text{Si}\{-^1\text{H}\}$ -CP-MAS NMR spectrum. According to the literature this signal can be assigned to a hexacoordinated silicon-fluoro-species.⁴⁰ Deconvolution of the quantitative $^{29}\text{Si}\{-^1\text{H}\}$ -MAS NMR spectrum shown in Fig. 4B was performed with DMFit software provided by Massiot *et al.*²⁵ Particularly noteworthy amongst the results of this analysis, which are summarized in Table 3, is that the calculated ratio of T-signal to the sum of the Q-signals amounts to 1 : 10.8. This value accurately reflects the APS : TEOS ratio of 1 : 10 used during synthesis (with respect to

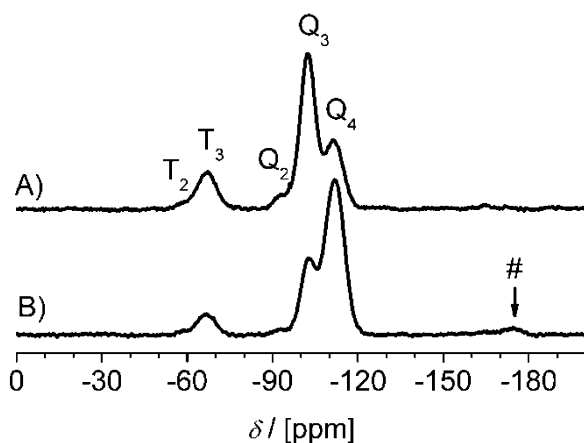


Fig. 4 Solid state $^{29}\text{Si}\{-^1\text{H}\}$ NMR spectra of a xerogel synthesized according to path B of Scheme 3. (A) Sensitivity enhanced $^{29}\text{Si}\{-^1\text{H}\}$ -CP-MAS NMR [7068 scans, contact time 3 ms, relaxation delay 3 s, measuring time 6 h]. (B) Quantitative $^{29}\text{Si}\{-^1\text{H}\}$ -MAS NMR [549 scans, relaxation delay 300 s, measuring time 2 days]. The signal labelled with the hash sign (#) originates from hexacoordinated silicon species.

the error of the method due to the signal to noise ratio of the spectrum). Further, the sole presence of T_3 -, Q_3 -, and Q_4 -signals with T_2 - and Q_2 -signal intensities being negligible shows that the siloxane network of the xerogel is highly condensed. The observed Q_3/Q_4 signal intensity ratio is 1 : 2.4, which means that more than 70% of the ethoxy groups of tetraethoxysilane were converted to $\equiv\text{Si}-\text{O}-\text{Si}\equiv$ bridges. The nearly complete absence of T_2 -signals indicates that virtually all methoxy groups of 3-aminopropyltrimethoxysilane are completely hydrolyzed and condensed.

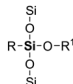
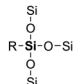
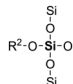
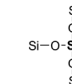
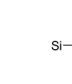
These conclusions are confirmed by the presence of ^{13}C NMR signals for non-hydrolyzed ethoxy groups of TEOS in the solid state $^{13}\text{C}\{-^1\text{H}\}$ -CP-MAS NMR spectra of the xerogels (Fig. 5). $^{13}\text{C}\{-^1\text{H}\}$ -CP-MAS NMR spectra of all xerogels were measured to confirm the formation of the desired *p*-nitroaniline-functionalized chromophore and its covalent attachment to the xerogel matrix. As exemplified in Fig. 5, all but two ^{13}C NMR signals that are observed originate from the *p*NA-functionalized chromophore. The two additional signals at 60 and 18 ppm (Fig. 5, signals 5 and 8, respectively) can be assigned to the non-hydrolyzed ethoxy groups of TEOS. No ^{13}C NMR signals commonly assigned to non-hydrolyzed CH_3O -groups of APS were detected, and neither were any ^{13}C NMR signals of residual 4-fluoronitrobenzene, which indicates high conversion rates and/or high efficiency of the purification procedure.

Quantitative determination of the chromophore content is achieved by dissolving a defined amount of dry xerogel in 1 M sodium hydroxide (NaOH) solution. When dissolved in 1 M NaOH the yellow coloured *p*-nitroaniline derivative shows a strong UV/Vis absorption at 416 nm. In the case of xerogels it is more practical to determine their mass-related extinction coefficient or mass-related chromophore content, F , instead of their molar extinction coefficient, ϵ , since their real molecular weight differs from their nominal molecular weight (eqn (1); refer to eqn (S1) in the ESI† for details on how to calculate ϵ):

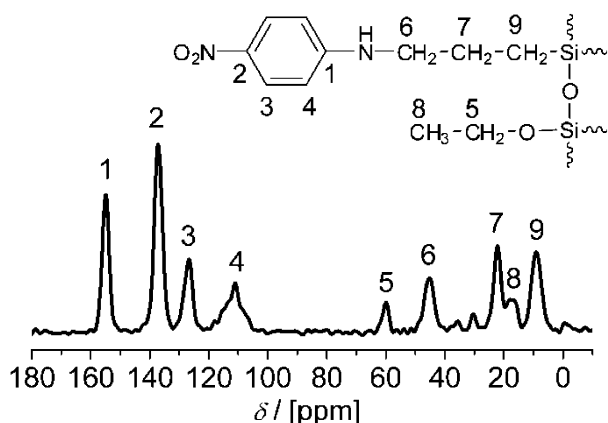
$$F = \frac{EV}{md} = \frac{\epsilon}{M} \cdot \left[\frac{L}{\text{g cm}} \right] \quad (1)$$

The value F is directly proportional to the chromophore content in a solid xerogel and specific for each individual batch. It is only useful to compare the optical properties of xerogels containing identical chromophores as different chromophores may be influenced by the dissolution process in different ways. Table 4 summarizes the F -values that were determined for the various synthesized xerogels. The reproducibility of the chromophore content is very good as indicated by the low standard deviations. It should be noted that for the samples produced without using TEOS as the solvent during the $\text{S}_\text{N}\text{Ar}$ -reaction slightly lower F -values were found. This can be explained by small amounts of the yellow pigment precursor sublimating at higher temperature as observed for the reaction of 4-FNB and APS in the substance, which we discussed earlier. In order to determine the maximum F -value, F_{max} , for *p*-nitroaniline functionalized xerogels with a chromophore-TEOS ratio of 1 : 10 the model compound *N*-propyl-4-nitroaniline (**M1**) was synthesized. Based on the molar extinction coefficient of this purely organic chromophore ($\epsilon = 21\,270 \text{ L mol}^{-1} \text{ cm}^{-1}$) and the “ideal” molecular weight of 1 : 10 xerogels ($832.12 \text{ g mol}^{-1}$), F_{max} can be as high as $25 \text{ L g}^{-1} \text{ cm}^{-1}$. The discrepancies between F_{max} and experimental F -values

Table 3 Quantitative analysis of the solid state $^{29}\text{Si}\{-^1\text{H}\}$ -MAS NMR spectrum shown in Fig. 4B by the structure of silicon species^a

^{29}Si NMR signal	T ₂	T ₃	Q ₂	Q ₃	Q ₄
Structure					
Chemical shift/ppm	-59.0	-66.0	-93.0	-103.0	-112.0
Percentage found	n.d.	8.5%	27.0%	n.d.	64.5%

^a R = $-(\text{CH}_2)_3\text{NHC}_6\text{H}_4\text{NO}_2$; R¹ = -H, -OMe; R² = -H, -OEt.

**Fig. 5** $^{13}\text{C}\{-^1\text{H}\}$ -CP-MAS NMR spectrum of a xerogel synthesized according to path B of Scheme 3 [TEOS used as solvent during the $\text{S}_{\text{N}}\text{Ar}$ -reaction, 4-FNB : APS : TEOS = (1 : 1 : 1) + 9/150 °C/5 h] and assignment of the ^{13}C NMR signals to the molecular structure [59 912 scans].

obtained for the as-synthesized xerogels originate from a higher “real” molar mass observed for the xerogels as discussed above, *i.e.* due to the incomplete sol–gel process, incomplete conversion of $\text{S}_{\text{N}}\text{Ar}$ -reaction, or maybe a loss of the organic chromophore during the long extraction with acetone. Table 4 further lists the specific surface area values of the xerogels as calculated from nitrogen adsorption measurements using the Brunauer–Emmett–Teller (BET) method.

Lastly, the morphology of selected xerogels was studied by electron microscopy techniques. Typical scanning electron microscopy (SEM) and transmission electron microscopy (TEM) images of as-obtained xerogels are shown in Fig. 6. Generally, spherical particles approximately 1 μm in size were obtained, although it must be noted that the particles did not exhibit a strictly monodisperse size distribution. The spherical particles tend to adhere to each other to form larger aggregates.

Thermal and pH-stability of *p*-nitroaniline functionalized xerogels

Thermal stability of the xerogels was studied using thermogravimetry (TG) as well as UV/Vis absorbance spectroscopy. The results of the thermogravimetric analyses of the various xerogels were very similar to one another. Fig. 7 exemplifies the general trend observed when heating *p*NA-xerogels. About 4% weight loss is observed up to a temperature of 200 °C due to the desorption of residual solvents and gases as well as the liberation of ethanol and water from hydrolysis and condensation reactions of previously uncondensed ethoxy groups within the silica matrix. Decomposition of the organic moiety commences at approximately 300 °C (see also ESI, Table S1†). UV/Vis absorption studies of heat-treated xerogels revealed that the optical properties of the chromophore change significantly once the temperature rises above 200 °C as evidenced by a significant decrease of the *F*-value beyond this temperature (Fig. 8 and ESI, Fig. S1†). This drop in the *F*-value is also in agreement with the change in visible appearance of the xerogels above this temperature (Fig. 8, inset).

para-Nitroaniline moieties encapsulated within the xerogels are resistant to strong aqueous acids such as hydrochloric acid (HCl). The yellow colour of the xerogel powders is not affected when they are treated with concentrated 6 M HCl solution over extended periods of time (*i.e.*, a few months). This clearly indicates that the dye is shielded from external influences by the silica matrix despite its porosity. In contrast, the colour intensity of the “unprotected” *p*NA-chromophore obtained after dissolution of the xerogel in aqueous NaOH is strongly pH-dependent as shown in Fig. 9. However, the actual wavelength of the UV/Vis absorbance maximum, λ_{max} , is almost unaffected by the pH value since only a small hypsochromic shift of 5 nm can be observed for λ_{max} when the pH changes from strongly basic to strongly acidic conditions (see ESI, Fig. S2†). The dissolved chromophore is accessible for protonation at the aniline nitrogen atom, which neutralizes the colour-causing push–pull system of the

Table 4 Variation of *para*-nitroaniline xerogel syntheses and corresponding mass related extinction coefficients (*F*) as calculated from UV/Vis absorption measurements, specific surface areas (S_{BET}) as calculated from N_2 -sorption measurements and the number of experiments (*n*) performed

Route	EtOH : water	$F/L \text{ g}^{-1} \text{ cm}^{-1}$	$S_{\text{BET}}/\text{m}^{-2} \text{ g}^{-1}$	<i>N</i>
Route A (without solvent during $\text{S}_{\text{N}}\text{Ar}$ -reaction, 4-FNB : APS : TEOS = (1 : 1 : 0) + 10/130 °C/5 h)	10 : 1	18.7 ± 1.2	440 ± 27	3
	3 : 1	18	400	1
Route B (one equivalent TEOS as solvent during $\text{S}_{\text{N}}\text{Ar}$ -reaction, 4-FNB : APS : TEOS = (1 : 1 : 1) + 9/130 °C/5 h)	10 : 1	19.4 ± 0.9	426 ± 80	9
Route B + higher temperature (one equivalent TEOS as solvent during $\text{S}_{\text{N}}\text{Ar}$ -reaction, 4-FNB : APS : TEOS = (1 : 1 : 1) + 9/150 °C/5 h)	10 : 1	20.2 ± 1.0	370 ± 38	4
	30 : 1	20	340	1

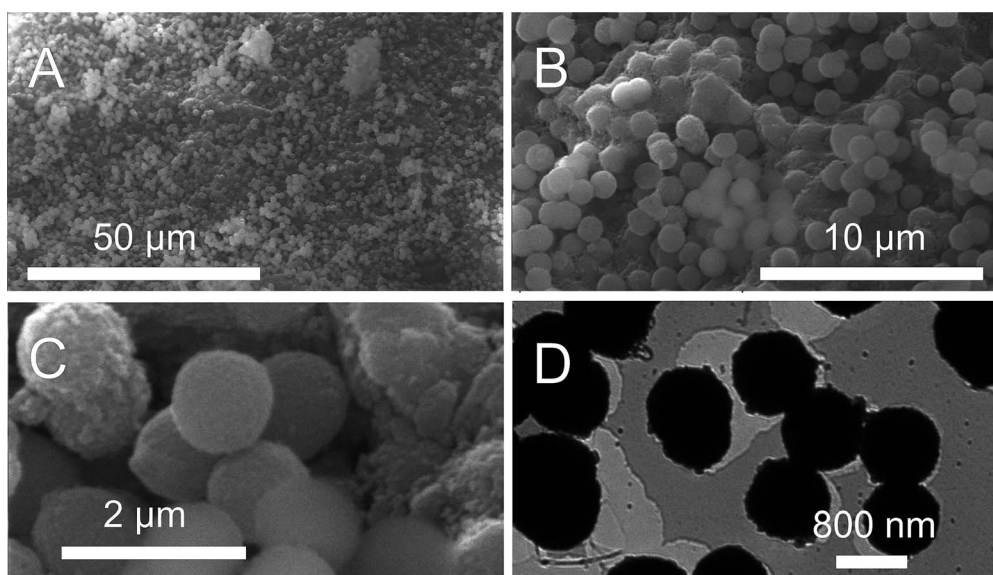


Fig. 6 Electron micrographs of a xerogel synthesized according to pathway A of Scheme 3 [no solvent during the S_NAr -reaction, 4-FNB : APS : TEOS = (1 : 1) + 10/130 °C/5 h]. (A–C) Scanning electron microscopy images at various magnifications and (D) transmission electron microscopy image.

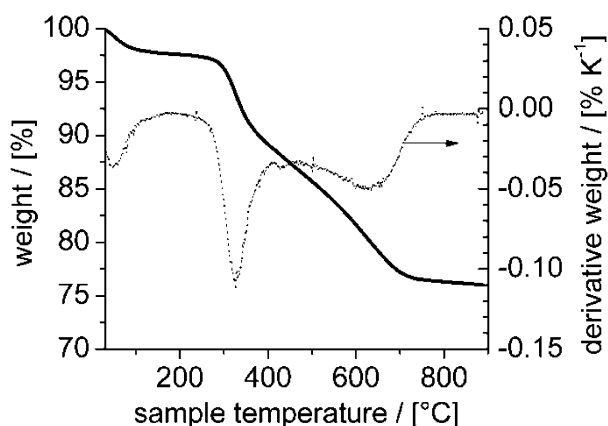


Fig. 7 Thermogravimetric analysis of a xerogel synthesized according to path B of Scheme 3 [TEOS used as solvent during the S_NAr -reaction, 4-FNB : APS : TEOS = (1 : 1 : 1) + 9/150 °C/5 h]. TG analysis was performed in air between 40 and 900 °C [heating rate: 10 K min⁻¹].

chromophore (Fig. 9, inset). This also explains why the colour of the model compound **M1** vanishes immediately when subjected to 6 M HCl solution.

Increasing the monodispersity of *p*-nitroaniline functionalized xerogels

The industrial application of *p*NA-functionalized xerogels as pigments requires a high degree of monodispersity of the particles with respect to their size. A well-studied process that produces uniform particles in the submicron range is the Stöber process.⁴¹ In a slight variation of our one-pot synthesis procedure we produced the chromophoric *p*-nitroaniline functionalized trimethoxysilane as described above (path B in Scheme 3), but instead of adding the residual TEOS to the reaction mixture after the completion of the S_NAr -reaction it was used to synthesize silica nanoparticles by the method of Stöber. Mixing the Stöber

particles with the chromophoric trimethoxysilane resulted in chromophoric core-shell particles containing a solid silica core (white) and a yellow coloured xerogel shell (Scheme 4).

Electron microscopy of the yellow powders revealed uniform particles with diameters of 180–190 nm (Fig. 10), which is significantly smaller than the xerogel particles obtained *via* our conventional route (1 μm). The mass related extinction

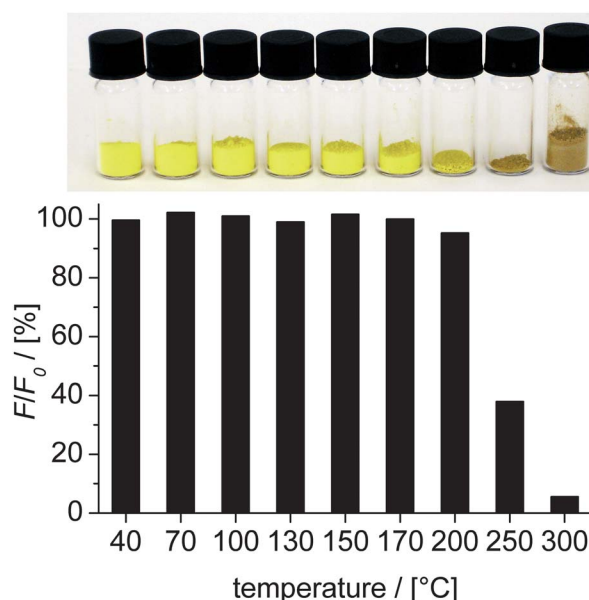


Fig. 8 Thermal stability of xerogels according to their UV/Vis characterization. The mass related extinction coefficient of *p*-nitroaniline xerogels, F , was determined after treating the xerogels at the indicated temperatures for five hours under reduced pressure (5 mbar). The observed significant decrease in F/F_0 at temperatures of 200 °C and above is supported by a change in visual appearance of the sample (photographs above each bar show the visual appearance after five hours of heat-treatment at the indicated temperatures).

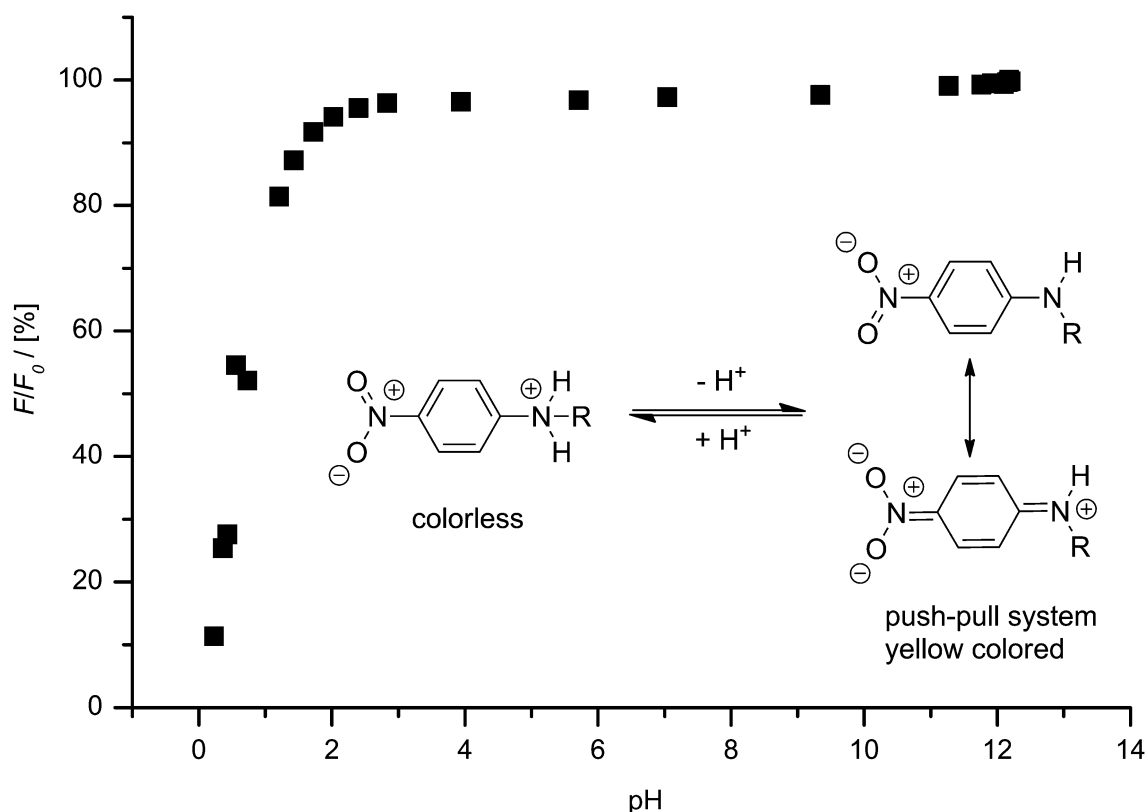


Fig. 9 The mass related extinction coefficient of dissolved *p*-nitroaniline xerogels as a function of the pH-value. The inset shows how protonation of the aniline nitrogen atom destroys the push–pull system responsible for the yellow colour of the chromophore [R = (CH₂)₃Si(OH)₃]. *F*₀ corresponds to the *F*-value measured immediately after the dissolution of the xerogels in caustic soda.

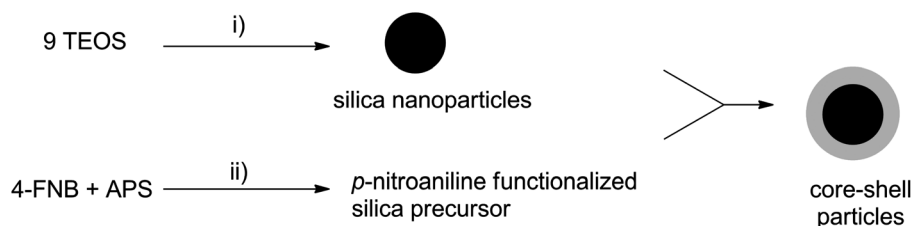
coefficient of the core–shell xerogels was determined to be 18 L g^{−1} cm^{−1}, which agrees very well with that of the other 1 : 10 xerogels (Table 4) proving that the conversion is quantitative. It is noted that the dissolution of these core–shell particles in aqueous NaOH occurs on a much slower timescale than that of the other xerogels, which indicates that the organically modified xerogel-shell shields the “Stöber”-silica core to a small extent from external influences such as NaOH solution. Additionally, the chromophores in the shell are still well protected against acidic conditions as discussed previously, and no decolourization of the particles was observed when they were stored in concentrated 6 M HCl solution over extended periods of time.

The expected homogeneity for the core–shell particles is also reflected in their nitrogen adsorption–desorption isotherms, and the type of isotherm found for these particles is typical for dense and non-porous materials (Fig. 11).

In comparison, xerogels prepared by the one-pot procedure show a hysteresis of type H2 that is typical for sol–gel derived silica materials exhibiting irregular pore shapes.⁴² The specific surface area (*S*_{BET}) and pore morphologies were determined by means of the BET and Dollimore–Heal method, respectively. The specific surface area of the core–shell particles (32 m² g^{−1}) is significantly lower than that of xerogels obtained using the one-pot procedure (567 m² g^{−1}). The low absolute value for the core–shell particles basically indicates that almost no porosity (*i.e.*, micro/mesopores) is observed for those particles.

Increasing the colour intensity of *p*-nitroaniline functionalized xerogels

As elucidated in the introduction the application of *para*-nitroaniline functionalized xerogels as pigments calls for highly stable



Scheme 4 Synthetic concept for the preparation of chromophoric core–shell particles. (i) Sol–gel process according to Stöber; (ii) S_NAr-reaction in TEOS as solvent corresponding to step 1 of both pathways in Scheme 2.

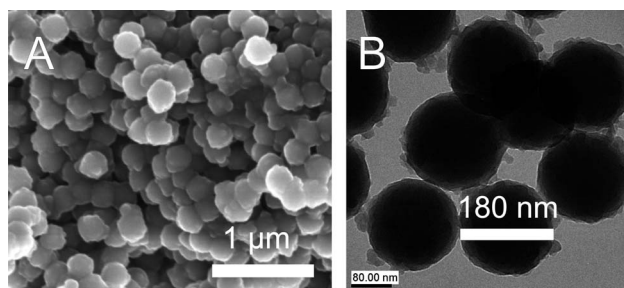


Fig. 10 (A) SEM and (B) TEM images of core-shell particles [scale bar: 1 μm and 180 nm, respectively].

and monodisperse xerogels, which are able to withstand a variety of chemical and mechanical stresses, while at the same time maximum colour intensity needs to be realized using minimal quantities of the materials. Increasing the chromophore content of xerogels can be accomplished in two ways: (i) by reducing the TEOS amount used during the one-pot synthesis or (ii) by replacing APS, which has only one amino group, with trialkoxysilanes bearing two or more amino groups such as 3-(2-aminoethylamino)propyltrimethoxysilane (DAS) and (3-trimethoxysilylpropyl)diethylenetriamine (TAS). We synthesized an

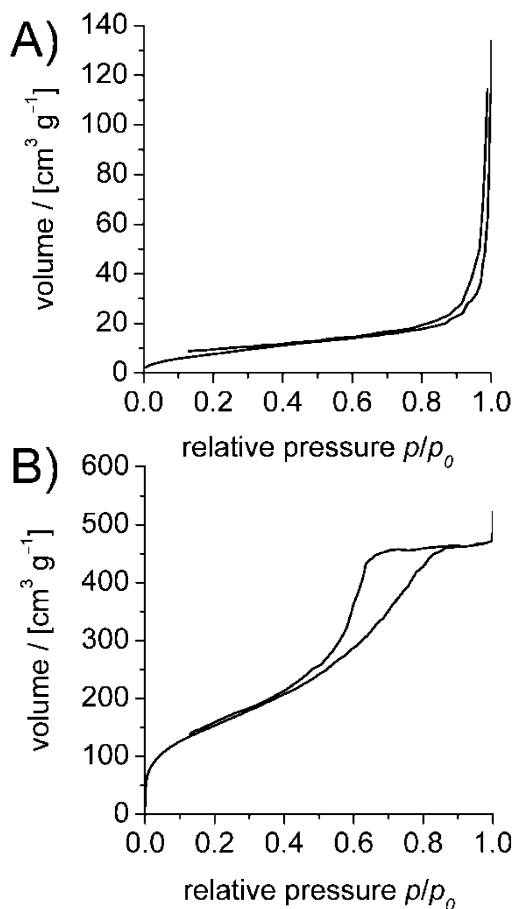


Fig. 11 Nitrogen adsorption and desorption isotherms of (A) core-shell particles and (B) of a xerogel obtained following synthesis procedure B as described in Scheme 3 [TEOS used as solvent during the $\text{S}_{\text{N}}\text{Ar}$ -reaction, 4-FNB : APS : TEOS = (1 : 1 : 1) + 9/130 $^{\circ}\text{C}$ /5 h].

array of *p*NA-functionalized xerogels using APS, DAS, and TAS as aminotrialkoxysilanes under variation of the aminotrialkoxysilane : TEOS ratio from 1 : 10 over 1 : 5 to 1 : 1 and analyzed the impact of both parameters on the F -value as well as some other physico-chemical properties of the xerogels. Chart 1 shows the chemical structures of the three aminotrialkoxysilanes used as well as those of their respective model substances, which were synthesized to calculate the F_{max} value for each xerogel variation and simplify data interpretation. Molecular weight, absorbance maximum, molar extinction coefficient, and F -value are given next to the structure of each model compound. F_{max} values given next to the structures of the aminotrialkoxysilanes correspond to values for xerogels with a aminotrialkoxysilane : TEOS ratio of 1 : 10, 1 : 5 or 1 : 1 from top to bottom, in that order. In the case of DAS and TAS xerogels the values given in brackets refer to the F_{max} values of mono- or mono-/di-substitution products, respectively.

Although the colour intensity (hence the F -value) increases with increasing number of available amino groups (Table 5), the experimental F -values differ quite significantly from the theoretical F_{max} values displayed in Chart 1. We therefore assume that not all available amino groups of DAS and TAS are converted during the $\text{S}_{\text{N}}\text{Ar}$ -reaction and only monosubstitution is achieved in the case of DAS and di-substitution in the case of TAS. This hypothesis is supported by the almost similar F -values for DAS and APS xerogels and the close to twice as high F -values for TAS xerogels. Even longer reaction times and higher reaction temperatures such as 20 h at 160 $^{\circ}\text{C}$ for the reaction of 4-FNB with DAS and 90 h at 180 $^{\circ}\text{C}$ for the reaction of 4-FNB with TAS did not significantly increase the F -values of the final products. It seems that the substitution reaction of the secondary amine group of DAS is sterically hindered if the primary group (from which it is only separated by one ethylene group) has already been converted to a *para*-nitroaniline moiety.

However, in the case of TAS being the nucleophile, di-substitution at the additional secondary amine group (which is closest to the silicon atom) is possible. Here, prior conversion of the primary group to a *p*NA moiety causes less steric hindrance because it is further away. Further, it is noted that the dissolution of DAS- and TAS-xerogels in caustic soda solution takes much longer than that of APS-based xerogels and in some cases complete dissolution cannot be achieved at all. This is, however, a critical observation since determination of the F -value *via* the method described above fails in the latter case and the measured F -value will be underestimated even if only a minor amount of the xerogel does not dissolve. In the cases where complete dissolution of the monosubstituted DAS-based xerogels was achieved the slower dissolution rate by still giving similar F -values shows that the organic chromophore of monosubstituted DAS-based xerogels is better protected against aggressive chemicals than that of APS-derived xerogels. Solid state ^{13}C - $\{^1\text{H}\}$ -CP-MAS NMR spectroscopy cannot distinguish between mono- and disubstitution of DAS xerogels or mono-, di-, and trisubstitution of TAS xerogels due to the overlapping NMR signals in combination with the lower resolution of solid state ^{13}C NMR spectroscopy compared to liquid NMR techniques (see ESI, Fig. S3 and S4†). Elemental analysis was not able to reveal the proper substitution state either because the differences in nitrogen and carbon contents between mono-, di-,

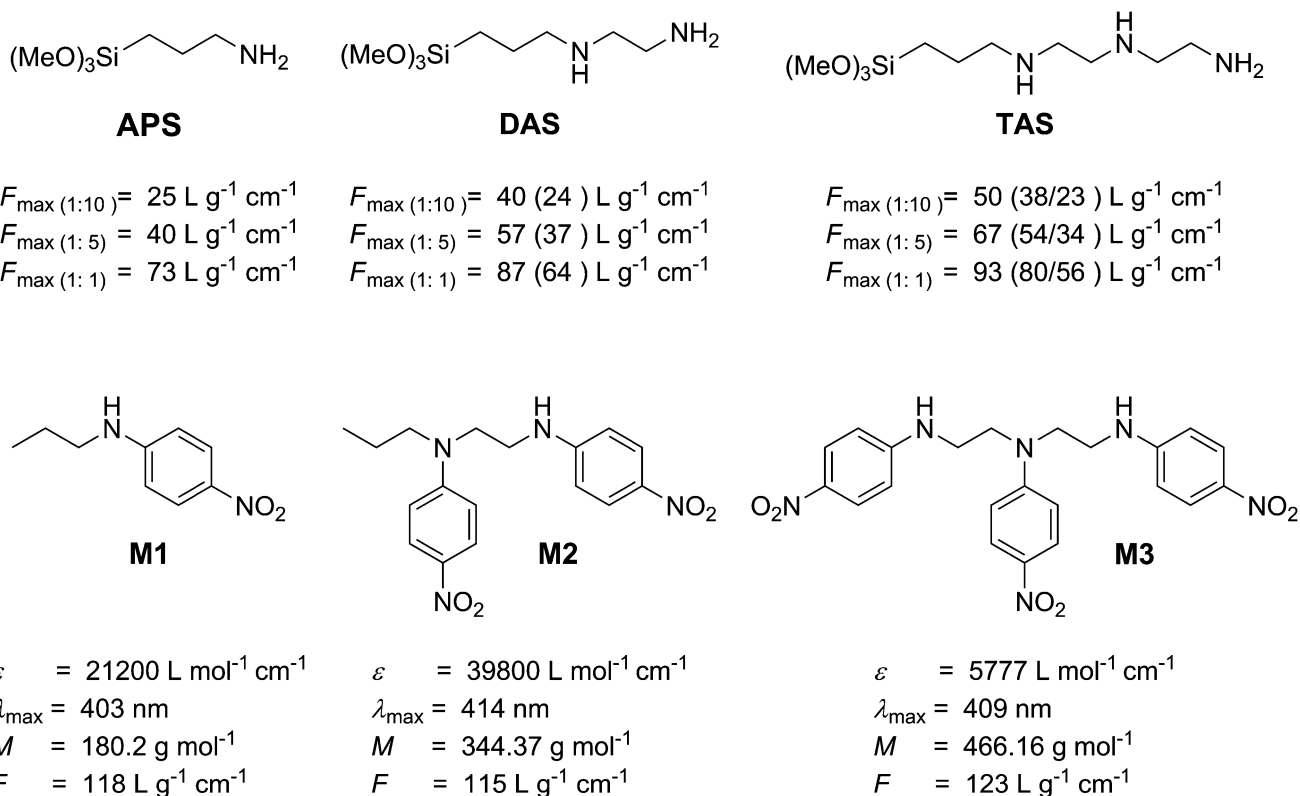


Chart 1 Chemical structures of mono-, di-, and tri-functional aminotrialkoxysilanes [APS: aminopropyltrimethoxysilane, DAS: 3-(2-aminoethylamino)propyltrimethoxysilane, TAS: (3-trimethoxysilylpropyl)diethylenetriamine] and corresponding model compounds **M1–M3**. Experimental UV/Vis spectroscopic characteristics of model compounds were obtained in DMSO [ϵ : molar extinction coefficient, λ_{\max} : wavelength of absorbance maximum, F -value: mass specific extinction coefficient, M : molecular weight]. Maximum possible F -values (F_{\max}) of APS-, DAS-, and TAS-derived xerogels were predicted based on aminosilane : TEOS ratios used (*i.e.*, 1 : 10, 1 : 5, and 1 : 1) and F -value of the corresponding model compound [values given in brackets refer to F_{\max} values for mono- or di-/mono-substituted products when using DAS or TAS, respectively].

and trisubstitution products are too small to confidently judge the rate of substitution. The previously described incomplete hydrolysis/condensation of TEOS during the sol–gel process skews the results of any elemental analysis even further.

The majority of the xerogels that were obtained using DAS or TAS as aminotrialkoxysilane showed a similar morphology to APS-derived xerogels in that they consisted of spherical particles approximately 1 μm in diameter. The specific surface area of DAS- or TAS-based xerogels as measured by N_2 -adsorption is very similar to that of the APS-derived powders for all trialkoxysilane : TEOS ratios studied (Table 5). Other physico-chemical properties of the xerogels such as their thermal stability are nearly unaffected by the increase in organic content that

accompanies the use of DAS or TAS as aminotrialkoxysilane. More precisely, the decomposition temperature of the organic moiety of the xerogels merely drops from 315 $^{\circ}\text{C}$ for APS-derived xerogels to 297 $^{\circ}\text{C}$ for TAS-derived xerogels.

The colour intensity obviously also increases with decreasing TEOS content of the reaction mixture (Table 5), but again, the theoretical F_{\max} values were not achieved (Chart 1). A decrease in the amount of TEOS used during the synthesis produces smaller specific surface areas due to the lowered porosity of the materials. As shown in Table 5, variation of the aminotrialkoxysilane : TEOS ratio has a much larger effect on the specific surface area than variation of the number of available amino groups.

Table 5 Mass related extinction coefficients (F) and specific surface areas (S_{BET}) of xerogels derived from mono-, di-, and tri-functional aminotrialkoxy-silanes [APS, DAS, TAS], 4-FNB, and TEOS [averaged values of multiple batches (n) are given]

Silane ^a Silane : TEOS ^b	APS			DAS			TAS		
	1 : 10	1 : 5	1 : 1	1 : 10	1 : 5	1 : 1	1 : 10	1 : 5	1 : 1
$F/\text{L g}^{-1} \text{ cm}^{-1}$	19 \pm 1	28 \pm 1	61 \pm 1	21 \pm 2	32 \pm 2	(>55) ^c	(>39) ^c	— ^c	— ^c
$S_{\text{BET}}/\text{m}^2 \text{ g}^{-1}$	410 \pm 65	120 \pm 50	<2	250 \pm 50	110 \pm 50	<2	260 \pm 30	80	<2
n	18	3	2	6	7	5	2	1	4

^a trialkoxysilane; ^b molar ratio of trialkoxysilane and TEOS; ^c not completely soluble in 1 M caustic soda solution.

The yellow-coloured pNA-xerogels were previously tested as pigments for the colouration of dental composite materials based on methacrylates which are commonly used for the restoration of teeth.⁴³ The mass of pigment required to obtain a desired colouration using the organic–inorganic xerogels is reduced by 96% compared to the formerly used pigment Yellow 53 (Lichtgelb 8G) resulting in improved optical properties of the composite such as transparency as well as superior mechanical properties.⁴⁴

Conclusions

Highly thermally and chemically stable, yellow-coloured xerogels were synthesized by combination of nucleophilic aromatic substitution reaction of 4-FNB with APS and a subsequently induced sol–gel process with TEOS as co-condensing silica source in a one-pot synthesis. Reaction parameters such as temperature, reaction time, concentrations and sol–gel conditions are systematically studied to optimize the conversion rate and reproducibility. We also prove for the first time that the HF formed during the S_NAr-reaction readily reacts with the silanes present in the reaction mixture, since it cannot be trapped by acid–base reactions, and catalyzes the subsequent sol–gel process. The materials can withstand temperatures of up to 200 °C and strongly acidic pH-conditions without any loss of colour. The chromophore is embedded in the silica matrix and therefore not accessible to strong acids that immediately decolourize a corresponding model compound by protonation. Further, core–shell particles with solid silica cores and chromophoric shells were produced. They exhibit the same dye content as our conventional xerogels, but combine it with more desirable monodisperse morphology and smaller particle diameters in the range of 200 nm. Finally, two convenient methods to enhance the colour intensity of the materials are presented. The main approach of increasing the number of available amino groups in the *n*-aminoalkyltrialkoxysilane leads to an increase in colour intensity (although steric hindrance prohibits full conversion of all amino groups) and enhanced chemical robustness, while other physicochemical properties remain almost identical. On the other hand, the far more obvious approach of decreasing the TEOS amount used in the synthesis also increases the colour intensity, but is accompanied by a drastic alteration of other properties such as the specific surface area.

Acknowledgements

Financial support by the Deutsche Forschungsgemeinschaft (DFG) and the Fonds der Chemischen Industrie is gratefully acknowledged. The authors thank M. Berger, S. Ebert, and D. Boettger-Hiller for nitrogen adsorption measurements, G. Baumann and S. Schulze for TEM/SEM imaging, and P. Schönherr for assistance with DSC/TGA measurements.

Notes and references

- R. J. Jeng, Y. M. Chen, A. K. Jain, J. Kumar and S. K. Tripathy, *Chem. Mater.*, 1992, **4**(5), 972–975.
- J. Kim, J. L. Plawsky, R. LaPeruta and G. M. Korenowski, *Chem. Mater.*, 1992, **4**(2), 249–252.
- F. Chaput, D. Riehl, Y. Levy and J. P. Boilot, *Chem. Mater.*, 1993, **5**(5), 589–591.
- S. C. Klein, *Sol–Gel Optics, Processing and Applications*, Kluwer Academic Press, Boston, 1994.
- C. Sanchez and F. Ribot, *New J. Chem.*, 1994, **18**(10), 1007–1047.
- Z. Yang, C. Xu, B. Wu, L. R. Dalton, S. Kalluri, W. H. Steier, Y. Shi and J. H. Bechtel, *Chem. Mater.*, 1994, **6**(10), 1899–1901.
- D. Avnir, *Acc. Chem. Res.*, 1995, **28**(8), 328–334.
- U. Schubert, N. Huesing and A. Lorenz, *Chem. Mater.*, 1995, **7**(11), 2010–2027.
- K. Yagi, S. Shibata, T. Yano, A. Yasumori, M. Yamane and B. Dunn, *J. Sol-Gel Sci. Technol.*, 1995, **4**(1), 67–73.
- F. Chaput, D. Riehl, J. P. Boilot, K. Cargnelli, M. Canva, Y. Levy and A. Brun, *Chem. Mater.*, 1996, **8**(2), 312–314.
- C. Sanchez and B. Lebeau, *Pure Appl. Opt.*, 1996, **5**(5), 689–699.
- J. Biteau, F. Chaput, K. Lahlil, J.-P. Boilot, G. M. Tsvigoulis, J.-M. Lehn, B. Darracq, C. Marois and Y. Levy, *Chem. Mater.*, 1998, **10**(7), 1945–1950.
- H. Jiang and A. K. Kakkar, *J. Am. Chem. Soc.*, 1999, **121**(15), 3657–3665.
- R. J. P. Corriu, *Angew. Chem.*, 2000, **112**(8), 1432–1455.
- J. A. Reyes-Esqueda, A. Franco, M. Bizarro, J. García-Macedo, M. Canva, B. Darracq, Y. Levy, K. Lahlil, F. Chaput and J. P. Boilot, *J. Sol-Gel Sci. Technol.*, 2003, **26**(1), 1011–1016.
- P. Gomez-Romero and C. Sanchez, *Functional Hybrid Materials*, Wiley-VCH Verlag GmbH, Weinheim, 2004.
- J. Bujdak and N. Iyi, *J. Phys. Chem. B*, 2006, **110**(5), 2180–2186.
- A. Seifert, K. Ladewig, P. Schönherr, K. Hofmann, R. Lungwitz, I. Roth, A. Pohlars, W. Hoyer, G. Baumann, S. Schulze, M. Hietschold, N. Moszner, P. Bartscher and S. Spange, *J. Sol-Gel Sci. Technol.*, 2010, **53**(2), 323–341.
- S. Spange, A. Seifert, H. Müller, S. Hesse and C. Jäger, *Angew. Chem., Int. Ed.*, 2002, **41**(10), 1729–1732.
- A. Seifert, S. Spange, H. Müller, S. Hesse and C. Jäger, *J. Sol-Gel Sci. Technol.*, 2003, **26**(1), 77–81.
- K. Schreiter, K. Hofmann, A. Seifert, A. Oehlke, K. Ladewig, T. Rüffer, H. Lang and S. Spange, *Chem. Mater.*, 2010, **22**(9), 2720–2729.
- I. Roth, F. Simon, C. Bellmann, A. Seifert and S. Spange, *Chem. Mater.*, 2006, **18**(20), 4730–4739.
- C. R. Morcombe and K. W. Zilm, *J. Magn. Reson.*, 2003, **162**(2), 479–486.
- R. Joseph, S. Zhang and W. T. Ford, *Macromolecules*, 1996, **29**(4), 1305–1312.
- D. Massiot, F. Fayon, M. Capron, I. King, S. L. Calvé, B. Alonso, J.-O. Durand, B. Bujoli, Z. Gan and G. Hoatson, *Magn. Reson. Chem.*, 2002, **40**(1), 70–76.
- C. E. S. Alvaro and N. S. Nudelman, *J. Phys. Org. Chem.*, 2005, **18**(8), 880–885.
- H. Grube and H. Suhr, *Chem. Ber.*, 1969, **102**(5), 1570–1579.
- J. Sauer and R. Huisgen, *Angew. Chem.*, 1960, **72**(9), 294–315.
- C. Claude, B. Garetz, Y. Okamoto and S. Tripathy, *Mater. Lett.*, 1992, **14**(5–6), 336–342.
- J. M. Allen, S. L. Aprahamian, E. A. Sans and H. Shechter, *J. Org. Chem.*, 2002, **67**(11), 3561–3574.
- R. Tacke, J. Becht, A. Lopez-Mras, W. S. Sheldrick and A. Sebal, *Inorg. Chem.*, 1993, **32**(12), 2761–2766.
- R. Tacke, J. Becht, A. Lopez-Mras and J. Sperlich, *J. Organomet. Chem.*, 1993, **446**(1–2), 1–8.
- R. Tacke, A. Lopez-Mras, W. S. Sheldrick and A. Sebal, *Z. Anorg. Allg. Chem.*, 1993, **619**(2), 347–358.
- R. Tacke, J. Becht, O. Dannappel, R. Ahlrichs, U. Schneider, W. S. Sheldrick, J. Hahn and F. Kiesgen, *Organometallics*, 1996, **15**(8), 2060–2077.
- A. Adima, C. Bied, J. Moreau and M. Wong Chi Man, *Eur. J. Org. Chem.*, 2004, (12), 2582–2588.
- R. J. P. Corriu, C. Guerin, B. J. L. Henner and W. W. C. Wong Chi Man, *Organometallics*, 1988, **7**(1), 237–238.
- J. A. Deiters and R. R. Holmes, *J. Am. Chem. Soc.*, 1990, **112**(20), 7197–7202.
- R. R. Holmes, *Chem. Rev.*, 1990, **90**(1), 17–31.
- C. J. Brinker and G. W. Scherer, *Sol–Gel Science: the Physics and Chemistry of Sol–Gel Processing*, Academic Press, San Diego, 6th edn, 1995.
- G. Hartmeyer, C. Marichal, B. Lebeau, P. Caullet and J. Hernandez, *J. Phys. Chem. C*, 2007, **111**(18), 6634–6644.

-
- 41 W. Stöber, A. Fink and E. Bohn, *J. Colloid Interface Sci.*, 1968, **26**(1), 62–69.
- 42 S. J. Gregg and K. S. Sing, *Adsorption, Surface Area and Porosity*, Academic Press, London, 2nd edn, 1995.
- 43 N. Moszner and S. Klapdohr, *Int. J. Nanotechnol.*, 2004, **1**(1–2), 130–156.
- 44 S. Spange, N. Moszner, P. Bartscher and V. Rheinberger, Eur. Pat. Appl., DE 101 373 72, EP 1 281 383 B1, US 6,833,394 B2, 2003.